AIMS Mathematics, 11(1): 1777–1806.
DOI:10.3934/math.2026074
Received: 07 October 2025
Revised: 15 December 2025
Accepted: 17 December 2025
Published: 20 January 2026

https://www.aimspress.com/journal/Math

Research article

Robust passivity-based boundary control of the 2-D Navier-Stokes equation with chaotic vortex

Fernando E. Serrano[1], **Vicenc Puig Cayuela**[2] **and Jesus M. Munoz-Pacheco**[3,*]

[1] Instituto de Robótica e Informática Industrial IRI-CSIC, Universidad Politécnica de Cataluña, Barcelona, España

[2] Automatic Control Department, Technical University of Catalonia (UPC), Rambla Sant Nebridi 22, 08222 Terrassa, Spain

[3] Faculty of Electronics Sciences, Benemérita Universidad Autónoma de Puebla (BUAP), Puebla 72570, Mexico

* **Correspondence:** Email: jesusm.pacheco@correo.buap.mx; Tel: +52-222-229-5500.

Abstract: This work introduced a novel control strategy for the chaos suppression in a numerical wave tank with chaotic vortices. The control strategy is based on designing a robust passivity-based boundary control for the uncertain Navier-Stokes equation interacting with a wave energy converter. First, the dynamic analysis of the uncertain Navier-Stokes equation was presented by determining the eigenfunction and eigenvalues along with computing the phase portraits, bifurcation diagrams, and Lyapunov exponents. Additionally, the proposed boundary controller was derived by selecting an appropriate Lyapunov functional, aiming to suppress the chaotic vortices present in the uncertain Navier-Stokes equation. In addition to the theoretical and numerical results, we also numerically evaluated the interactions between an energy wave converter generator and the chaotic vortices, first as an open-loop problem, and next, the proposed boundary control strategy was tested to suppress the chaotic behavior. Finally, the discussion and conclusion of this research study were presented.

Keywords: chaotic vortex; chaotic systems; Navier-Stokes equation; port-Hamiltonian formulation; passivity-based control
Mathematics Subject Classification: 35Q30, 37J65, 37M05, 65P10, 76F70

1. Introduction

As is known, chaotic phenomena are found in many kinds of physical systems, which are described as dynamical systems in integer-order or fractional-order domains. Among these kinds of systems are electrical, mechanical, biological, and chemical ones. In recent years, chaotic behavior has also been

observed in systems described by partial differential equations, such as fluid, optical, electromagnetic, and quantum systems. Therefore, the interest in studying chaotic systems described by partial differential equations has recently increased. In the meantime, the port-Hamiltonian formulation for partial differential equations is an attractive tool due to its advantages in expressing the energy and structure of a dynamical system based on partial differential equations.

This research paper aims to explore and examine the chaotic phenomena in fluid systems governed by the Navier-Stokes equations. Then, we present a literature survey of analytical and numerical solutions for the Navier-Stokes equation. Reference [1] presented the global solution of the 3D Navier-Stokes equation. The Navier-Stokes equation for a phase-field crystal system was analyzed in [2]. The weak solution of the Navier-Stokes equation with minor regularity was then demonstrated in [3]. The Rayleigh-Stokes equations were explored using the finite element approach in [4], and the conditional regularity of the Navier-Stokes equation was shown in [5].

Some references related to chaos-based video encryption techniques have also been given. For instance, in [6], a video encryption strategy for the discrete sinusoidal memristive Rulkov neuron was presented. In [7], a pseudorandom generator and video encryption strategy were given, in which a three-dimensional memristive hyperchaotic system was employed. Then, in [8], a chaos-based video-encryption technique was also presented.

Other related research studies can be found in references such as [9], where the weak solution of a Navier-Stokes equation was analyzed. Next, in [10], an essential reference for this research, a 2D Navier-Stokes equation was studied to investigate its periodic behavior. Meanwhile, in [11], the numerical solution of the Navier-Stokes equation by the finite element method was presented.

Additionally, several studies have examined chaotic fluid vortices. For instance, the multimodal motion dynamics of a top-tensioned riser triggered by vortices were demonstrated in [12]. The chaotic quantification in a vortex system was examined in [13] while ocean turbulence was studied in [14]. Also, the experimental observation of a chaotic vortex in a turbulent flow was presented in [15]. The dynamic study of a chaotic ellipsoidal vortex was then carried out in [16]. Reference [17] presented the numerical analysis of unsteady non-isothermal flows. Finally, in [18], the solution of the stationary Navier-Stokes equation was established.

In the meantime, several authors have presented the Navier-Stokes equation in the port-Hamiltonian formulation, arguing that it provides a compact formulation that offers an energetic and structural perspective for dynamic analysis, yielding improved results. For instance, fluid modeling and control using the port-Hamiltonian formulation was described in [19]. The port-Hamiltonian formulation of observed flows was then shown in [20]. In [21], an exergetic port-Hamiltonian formulation was used to model a Navier-Stokes-Fourier fluid. Then in [22], the incompressible Navier-Stokes equations were formulated as a port-Hamiltonian system.

Besides, in [23], the characteristics of a vortex found in a water pump were presented. In [24], a neural network was implemented to simulate a 3D turbulent flow. Then, in [25], the numerical study of laminar flow in fully wavy flow micro channels was presented. In [26], the hydrodynamic characteristics in oscillating feedback micromixers were introduced, and in [27], the flow dynamics behavior of a reactor was presented.

Other research studies regarding the port-Hamiltonian formulation can be found in [28], where a boundary-controlled port-Hamiltonian system using the backstepping control technique was presented. In [29], the model reduction of a distributed parameter system in the form of a port-Hamiltonian system

was studied. Meanwhile, in [30], the structure preserving a 1D distributed parameter system in the form of a port-Hamiltonian formulation was presented. Then, in [31], a discrete-time representation of a port-Hamiltonian system was given, while the learning of partial differential equations by quantified stochastic port-Hamiltonian systems was presented [32].

Given that new control techniques were herein applied to the 2D Navier-Stokes equation port-Hamiltonian formulation, passivity-based controllers are crucial for this research work. Since the uncertain port-Hamiltonian formulation is the primary focus of this work, it is worth noting that the literature has reported a small number of results. Most of the references listed dealt only with nominal distributed parameter port-Hamiltonian systems that were controlled by passivity [33–36]. The lumped parameter version and the passivity-based control for the distributed parameter port-Hamiltonian system share a similar nature. A storage function was designed as part of the passivity-based boundary control, and the passivity-based control law was then synthesized. In such cases, in [37], the vibration suppression of a flexible beam was realized by a passivity-based controller. In [38], the matching equations of kinetic energy shaping for interconnection and damping assignment-passivity-based control were given. In [39], the design of fault-tolerant and non-fragile control for parabolic port-Hamiltonian systems with semi-Markov chains was presented. In [40], adaptive energy-shaping control for a cable-driven underactuated parallel robot was presented.

It is important to note the differences and advantages of the proposed robust boundary control strategy in comparison with other control techniques for the stabilization of the Navier-Stokes equation. For example, the difference between the proposed control strategy and [41] lies in the use of a stochastic version of the Navier-Stokes equation and its associated optimal controller. As a result, the controller developed in [41] does not take into account uncertainties of any kind. In [42], different Reynolds numbers were considered for optimal control problems of the Navier-Stokes equation. The present study does not account for variations in Reynolds number, but it does account for uncertainties in the boundary conditions. It represents a significant insight in comparison with [42]. Meanwhile, in [43], results for the control of a 2D Navier-Stokes equation were presented, in which, in contrast to the present study, periodic and temporally steady forcing terms were considered. However, the port-Hamiltonian formulation surpasses a standard Navier-Stokes formulation, yielding a more robust controller because unmodelled dynamics were not accounted for in the latter. Then, in [44], the weak solution of a time fractional Navier-Stokes equation was given. It is important to note that an optimal controller was implemented in that reference. So the dissipative conditions of the Navier-Stokes equation presented in this research study were an advantage, facilitating the control of the Navier-Stokes equation in the port-Hamiltonian formulation.

Before presenting the theoretical and experimental insights of this work, we would like to outline a route map for the entire study, clarifying and detailing the path of the investigation.

- The main result of this research study is to find a chaotic or hyper-chaotic attractor in the 2D Navier-Stokes equation. To this end, the respective eigenvalues and Lyapunov exponents of the Navier-Stokes equation are found, as well as the bifurcation analysis.
- Another important goal of this research study is to develop a feasible and robust passivity-based controller that achieves optimal performance for chaos suppression in the 2D Navier-Stokes equation in its port-Hamiltonian formulation.
- The robust passivity-based controller is chosen taking into consideration the energy characteristics of the Navier-Stokes equation in the port-Hamiltonian form. Using the input-output attributes of

the distributed parameter port-Hamiltonian mathematical model, the appropriate control law is synthesized.

- A last objective is to determine whether the proposed robust boundary passivity-based controller eliminates and suppresses the chaotic and turbulent behavior of the water fluid to protect a wave energy converter. By employing a proportional derivative controller, the wave energy converter velocity is regulated to protect it both mechanically and electrically.

For those purposes, a comprehensive dynamic analysis is performed to find and analyze the eigenfunctions and eigenvalues of the system. Next, the phase portraits, bifurcation diagrams, and the respective Lyapunov exponents are derived. In addition, the uncertain port-Hamiltonian formulation of the 2D Navier-Stokes equation is obtained by selecting the appropriate Hamiltonian function, which facilitates the subsequent design of the boundary controller for chaos suppression.

Next, a robust passivity-based boundary controller is designed for the port-Hamiltonian system in order to stabilize the system and to generate the flow velocity used as a reference for the wave energy converter (WEC). The wave energy converter uses the flow potential velocity generated in a numerical wave tank (NWT) which results from the simulation of the 2D Navier-Stokes equation as a reference. Then this variable is tracked by a standard proportional-derivative (PD) controller for the (WEC). This means that, apart from suppressing chaos artificially in a numerical wave tank experimental setup, the shaft velocity of the wave energy converter is achieved by the implementation of a single PD controller. Then, the angular velocity of the shaft is regulated by considering the potential velocity vector of the water fluid. In this way, the WEC is protected mechanically by avoiding structural damage and electrically by avoiding exceeding the nominal power generated.

2. Theoretical background of the Navier-Stokes equation

The Navier-Stokes equation is a crucial theoretical formulation for modeling the flow and vorticity of various types of fluids. In this paper, it is shown how to use the Navier-Stokes equation to solve a chaotic vortex water fluid model in a numerical wave tank. As a result, we can simulate how to drive and protect a wave energy converter from chaotic turbulence by suppressing the chaotic behavior of water with a robust passivity-based boundary controller.

In the following subsections, the standard and Eulerian formulations of the Navier-Stokes equation are presented, which are later converted to an uncertain port-Hamiltonian formulation in this paper to facilitate the design of the proposed stabilization and chaos suppression strategy. Additionally, a comparative table of the different Navier-Stokes formulations, presented in both Eulerian and port-Hamiltonian forms, is provided.

2.1. Standard and Eulerian formulation of the Navier-Stokes equation

The standard formulation of the Navier-Stokes equation is obtained from Cauchy's differential equation of motion for incompressible and compressible fluids [45]:

$$\rho \frac{DU}{Dt} = \nabla.\sigma + \rho g, \tag{2.1}$$

in which U is the fluid velocity, ρ is the fluid density, g is the gravity vector, and σ is stress tensor. So the Navier-Stokes equation is obtained as shown below [45]:

$$\rho \frac{DU}{Dt} = -\nabla p + \mu \nabla^2 u + \rho g, \tag{2.2}$$

in which μ is the viscosity of the fluid. In the literature, some results regarding the solution of the Navier-Stokes equation have been found. For example, in [46], the blow-up criterion for the Navier-Stokes-Fourier equations was evinced. In [9], the L_2 decay of the weak solution of the Navier-Stokes equation was shown. In [47], the research on the aerodynamic drag by the Navier-Stokes formulation was presented. On the other hand, in [48], a two-phase flow was analyzed using the Navier-Stokes equation. Then, in [49], the boundary value problem for the solution of the Navier-Stokes equation with density-dependent viscosity was given.

The Eulerian formulation of the Navier-Stokes equation is fundamental for spatio-temporal analysis and transformation to the port-Hamiltonian formulation. The Eulerian formulation is given as:

$$\rho \left(\frac{\partial U}{\partial t} + u.\nabla u \right) = -\nabla p + \mu \nabla^2 u + \rho g, \tag{2.3}$$

where p is the pressure vector. Regarding the port-Hamiltonian formulation of the Navier-Stokes equation, various works can be found. In [19], the port-Hamiltonian formulation of fluid for dynamic modeling and control was evinced. In [50], the port-Hamiltonian formulation of continuum mechanics was discussed. In [20], the port-Hamiltonian formulation of ocean flow was presented. In [22], the incompressible Navier-Stokes equation in the port-Hamiltonian formulation was given. Finally, in [51], the geometric decomposition of the Navier-Stokes equation in the Port-Hamiltonian formulation was shown.

2.2. Analytic solutions of the Navier-Stokes equation

The analytic solution of the Navier-Stokes equation is crucial for this research study, as a partial solution is required to find the eigenfunctions and eigenvectors of this partial differential equation. In the following paragraph, we will show some results found in the literature regarding the weak or strong solution of the Navier-Stokes equation. As it is known, the solution of the Navier-Stokes equation depends on factors such as the dimension and boundary conditions. For instance, in [9], the $\mathcal{L}_2$ weak solution of the Navier-Stokes equation was presented. Reference [52] showed the strong solution of the 3D Navier-Stokes equation. Then, in [53], the time periodic strong solution of the incompressible Navier-Stokes equation was presented, and in [54], the two-variable solution of the Navier-Stokes equation was presented.

The eigenfunction and solution of the Navier-Stokes equation in this research paper are obtained using a method similar to that described in [54], which involves a separation of spatial and temporal variables.

One of the most interesting results is the strong solution of the Navier-Stokes equations as evinced in [52], which can be described as:

$$\begin{aligned} u_t + u.\nabla u + \alpha |u|^{\sigma-2} u + \nabla p &= \nabla.(S(\nabla u)), \\ \nabla.u &= 0, \end{aligned} \tag{2.4}$$

where $u \in \mathbb{R}^3$ is the velocity potential of the fluid. Based on the following initial condition [52]:

$$u(x, 0) = u_0(x), \tag{2.5}$$

the solutions are given by:

1) $S(\nabla u) = |\nabla u|^{q-2}\nabla u + \nabla u$.
2) $S(\nabla u) = |\nabla u|^{q-2}\nabla u$.

We refer readers to [52] for an extended derivation of both results.

3. Problem formulation

As explained before, the main problem to be solved in this research study is to suppress the chaos phenomenon in the port-Hamiltonian formulation of a numerical wave tank to protect a wave energy converter from the damage generated by a chaotic vortex. Therefore, the problem formulation section is established in two parts:

1) The 2D Navier-Stokes equations. These equations are important because the 2D numerical wave tank is represented by the Navier-Stokes equations. The numerical wave tank consists of a 2D grid in which the wave energy converter is tested.
2) The second part of the problem formulation consists of establishing the WEC dynamic behavior. In this way, the angular velocity of the WEC, along with the generated power, is computed to observe and protect the WEC from damage generated by the chaotic behavior of the fluid in the 2D confinement.

3.1. Navier-Stokes equations for the NWT

The Navier-Stokes equation used herein is a spatio-temporal 2D partial differential equation that is later converted into a port-Hamiltonian formulation. For these purposes, the appropriate Hamiltonian is implemented to obtain the required port-Hamiltonian formulation. Consider the following 2D Navier-Stokes partial differential equations in Eulerian form [45]:

$$\begin{aligned}
\rho\left(\frac{\partial u_x}{\partial t} + u_x\frac{\partial u_x}{\partial x} + u_y\frac{\partial u_x}{\partial y}\right) &= -\frac{\partial p}{\partial x} + \mu\left(\frac{\partial^2 u_x}{\partial x^2} + \frac{\partial^2 u_x}{\partial y^2}\right),\\
\rho\left(\frac{\partial u_y}{\partial t} + u_x\frac{\partial u_y}{\partial x} + u_y\frac{\partial u_y}{\partial y}\right) &= -\frac{\partial p}{\partial y} + \mu\left(\frac{\partial^2 u_y}{\partial x^2} + \frac{\partial^2 u_y}{\partial y^2}\right),
\end{aligned} \tag{3.1}$$

in which the components of the vector velocity field are given by $u = [u_x, u_y]'$, p is the pressure variable, ρ is the density constant, and μ is the viscosity constant that, in this case, is related to water. Numerical simulations are shown in Figures 1 and 2, respectively. It is worth noting that the uncertainties and boundary conditions are explained in detail later in Subsection 4.1. In this manner, the theoretical and experimental setup of the wave energy converter is given by:

1) Stabilization and chaos suppression by robust passivity-based boundary control.

2) Numerical wave tank for wave energy conversion simulation.

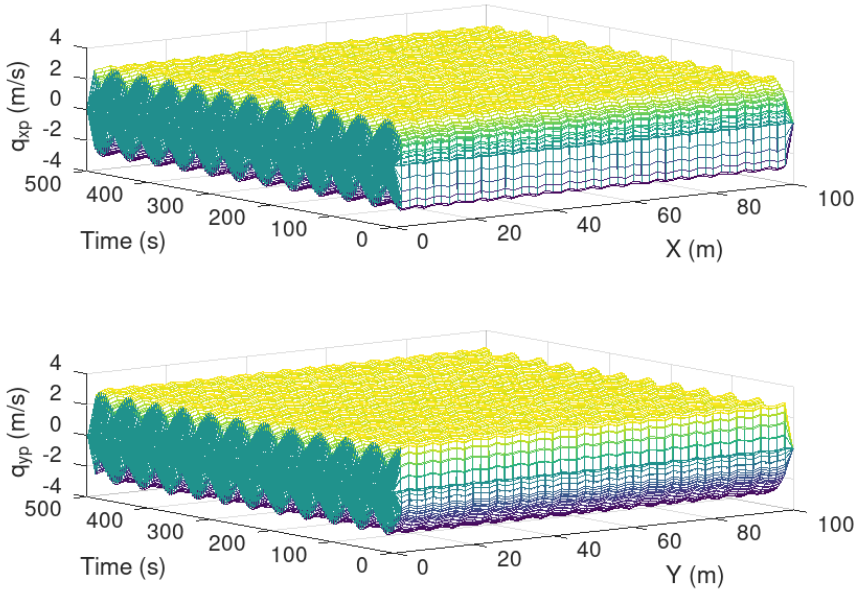

Figure 1. Mesh plot of the numerical wave tank by solving the 2D Navier-Stokes equations.

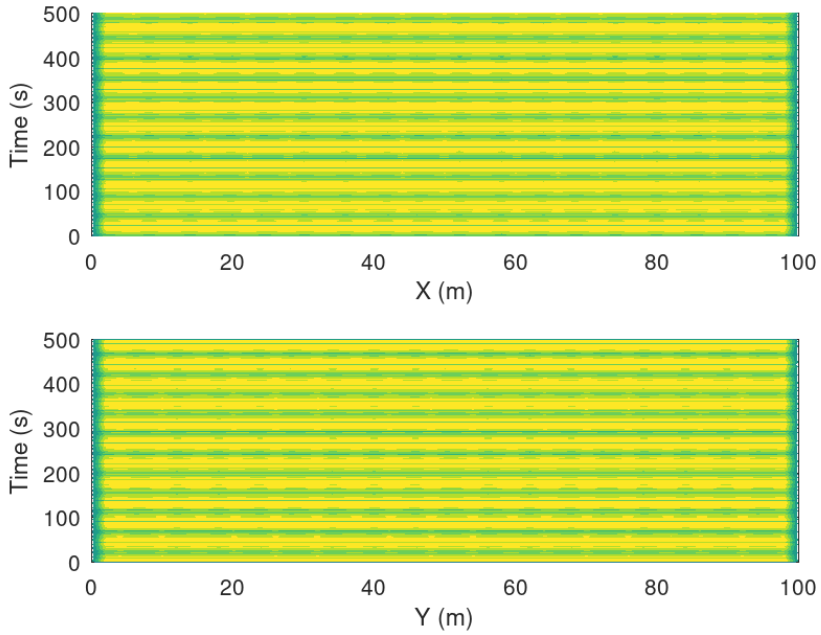

Figure 2. Contour plot of the numerical wave tank by solving the 2D Navier-Stokes equations.

Figure 3 shows the schematic diagram of the NWT setup implemented for the simulation of the

chaotic vortex. In Section 5, it is explained in detail how this numerical wave tank experimental setup is established by using real laboratory components:

- A water pump,
- A manometer to measure the water pressure,
- A water level meter in the x direction,
- A water level meter in the y direction,
- The passivity-based boundary controller,
- A voltage converter to transform the input value into a voltage for the pump.

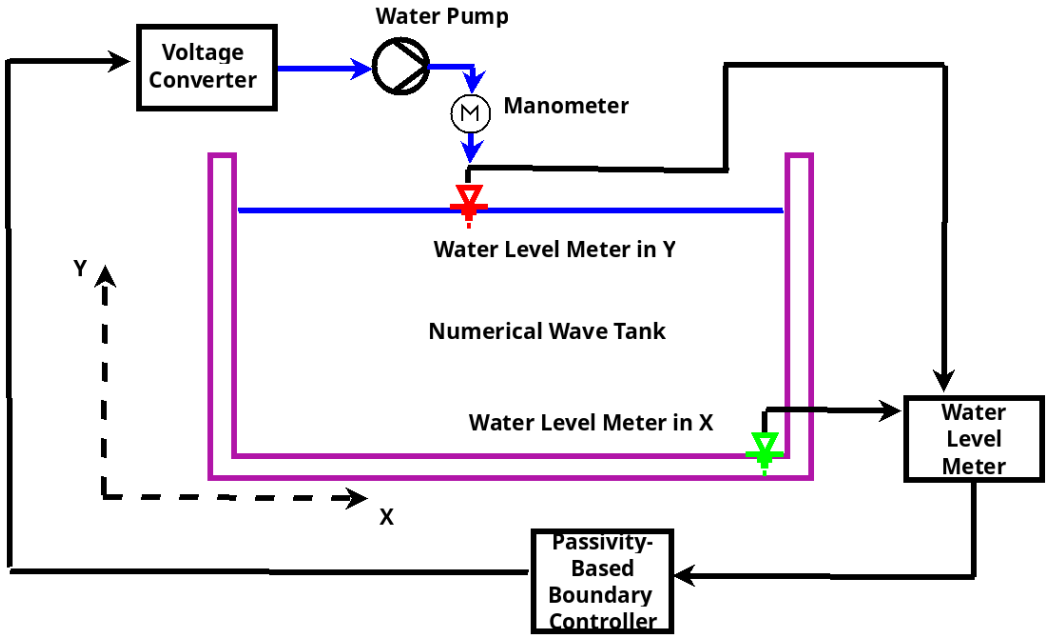

Figure 3. Numerical wave tank schematic diagram.

3.2. Wave energy converter formulation

The wave energy converter dynamics are detailed in Subsection 5.1. The wave energy converter dynamics are composed of:

1) Shaft angular velocity of the WEC.
2) Generated power of the WEC.

Although the dynamics of the WEC are relatively simple, they are crucial for the trajectory tracking of the WEC. This trajectory tracking consists of obtaining the norm of the fluid velocity potential as the desired angular velocity of the shaft. The relationship between the wave energy converter and the numerical wave tank serves as a mechanism to mitigate chaotic behavior within the tank. This suppresses chaos in the waves and protects the wave energy converter.

4. Stabilization and chaos suppression by robust passivity-based boundary control

The robust passivity-based boundary stabilization for chaos suppression in the numerical wave tank involves finding an appropriate boundary control law that considers the energy properties of the

uncertain port-Hamiltonian formulation. The variables implicated are given in Table 1.

Table 1. Variables in the Navier-Stokes equation in the uncertain port-Hamiltonian formulation.

Variable	Definition	Formula
q	This variable is the flow position with $\dot{q} = u$ as the velocity potential vector.	$q = [q_x, q_y]^T$
M_v	This variable is the volumetric momentum vector.	$M_v = [M_x, M_y]^T$
p	This variable is the pressure vector.	$p = [p_1, p_2]^T = [p_x \sin(X), p_y \cos(Y)]^T$
g	This variable is the gravity variable.	See Eq (4.1)
u_1, u_2, u_3, u_4	These variables are the boundary inputs.	See Eq (4.9)
$\eta_1, \eta_2, \eta_3, \eta_4$	These are the boundary uncertainties.	$\eta_1 = -sin(X)$, $\eta_2 = sin(Y)$, $\eta_3 = -cos(X)$, $\eta_4 = cos(Y)$

In Table 2, a quantitative comparative analysis of the proposed control strategy with other techniques found in the literature is presented.

Table 2. Comparative analysis of the proposed control strategy.

Reference	Advantages	Disadvantages
(Gao et al., 2025 A) [55]	The 2D formulation is appropriate and suitable for this research study.	Available only in a discrete time formulation.
(Gao et al., 2025 B) [56]	Available for three dimensions.	Not implementable for spatio-temporal analysis and available only in a discrete time formulation.
(Ma et al., 2025) [57]	Available for energy consumption and dissipation. Similar to the proposed control strategy.	Not available for spatio-temporal analysis.
(Shi et al., 2024) [58]	Available for multi-agent systems with delay. It is only applicable to stochastic systems.	

The gravity vector g in Table 1 is described by:

$$g = [9.81\cos(t), 9.81\sin(t)][0.3cos((2\pi 0.5)t), 0.3\sin((2\pi 0.5)t)]^T. \tag{4.1}$$

For the robust passivity-based stabilization, consider the following theorems.

Theorem 1. *Consider the control input $u \in \mathbb{R}^n$ and the output $y \in \mathbb{R}^n$, so the following storage function $V_s(x) : \mathbb{R}^n \to \mathbb{R}$ is implemented for robust passivity-based stability and the following is met [59]:*

$$\dot{V}_s(x) \leq \sum_{i=1}^{n} \alpha_i u_i y_i, \tag{4.2}$$

for $\alpha_i \in \mathbb{R}^+$, in which $u_i \in \mathbb{R}$ are the boundary control inputs and $y_i \in \mathbb{R}$ are the outputs of the port-Hamiltonian distributed parameter system.

Theorem 2. *Consider the following control variable $u \in \mathbb{R}^n$ and the output $y \in \mathbb{R}^n$, and the following storage function $V_s(x) : \mathbb{R}^n \to \mathbb{R}$ with the following α function $\alpha = x^2 + y^2$. To obtain robust passivity stability the following is required [60–64]:*

$$\underset{u\in U}{inf}\ \underset{x\in Q}{sup}[V_s(x, y, u, t) + \alpha(x, y)] \leq 0. \tag{4.3}$$

4.1. Uncertain representation of the Navier-Stokes equation in the port-hamiltonian formulation

Consider the following augmented state:

$$X = [q^T, M_v^T]^T, \qquad q = [q_x, q_y]^T, \qquad M_v = [M_{vx}, M_{vy}]^T, \tag{4.4}$$

and the following Hamiltonian:

$$H(q, M_v) = \frac{\rho}{2}\dot{q}^T\dot{q} - \int_q \nabla p^T dq + \mu \int_q \nabla^2 \dot{q}^T dq + \rho g^T q, \tag{4.5}$$

in which $M_v = \rho\dot{q}$, where M_v indicates the volumetric momentum. The multiplicative parametric uncertainty is given by:

$$\begin{bmatrix} \frac{\partial}{\partial t}q \\ \frac{\partial}{\partial t}M_v \end{bmatrix} = \underbrace{\begin{bmatrix} 0_n & I_n \\ -I_n & 0_n \end{bmatrix}}_{G} \underbrace{\begin{bmatrix} -\nabla p + \mu\nabla^2\dot{q} + \rho g \\ \dot{q} \end{bmatrix}}_{f}, \tag{4.6}$$

with the following boundary conditions, considering that the system variable trajectory is periodic:

$$\begin{aligned} \dot{q}_x(x, 0) &= u_1 + \eta_1, & q_x(x, 0) &= x, \\ \dot{M}_x(x, 0) &= u_2 + \eta_2, & M_x(x, 0) &= -x, \\ \dot{q}_y(y, 0) &= u_3 + \eta_3, & q_y(y, 0) &= y, \\ \dot{M}_y(y, 0) &= u_4 + \eta_4, & M_y(y, 0) &= -y, \end{aligned} \tag{4.7}$$

where the boundary uncertainty $\eta = [\eta_1, \eta_2]^T$ meets the following property.

Property 1. *Considering the boundary uncertainty η, the following property is met:*

$$\|\eta(x, y)\|_2 \leq \gamma, \tag{4.8}$$

in which $\gamma > 0$, so in other words $\eta(x, y)$ is bounded for all $t > 0$.

4.2. Theoretical derivations

To obtain the robust passivity-based boundary controller, the following theorem is needed:

Theorem 3. *Consider the following robust passivity-based control laws:*

$$\begin{aligned} u_1 &= \begin{cases} x-\eta_1 & \textbf{if} \quad x \neq 0, \\ -\eta_1 & \textbf{if} \quad x = 0, \end{cases} \\ u_2 &= \begin{cases} x-\eta_2 & \textbf{if} \quad x \neq 0, \\ -\eta_2 & \textbf{if} \quad x = 0, \end{cases} \\ u_3 &= \begin{cases} y-\eta_3 & \textbf{if} \quad y \neq 0, \\ -\eta_3 & \textbf{if} \quad y = 0, \end{cases} \\ u_4 &= \begin{cases} y-\eta_4 & \textbf{if} \quad y \neq 0, \\ -\eta_4 & \textbf{if} \quad y = 0, \end{cases} \end{aligned} \tag{4.9}$$

with output $y = [q_x, q_y, M_x, M_y]^T$ so system (4.6) is stabilized.

Proof. Consider the following storage function:

$$V = \frac{1}{2}\int_0^{L_x} q_x^2(x,0)dx + \frac{1}{2}\int_0^{L_y} q_y^2(y,0)dy + \frac{1}{2}\int_0^{L_x} M_x^2(x,0)dx + \frac{1}{2}\int_0^{L_y} M_y^2(y,0)dy. \tag{4.10}$$

So the first derivative of the previous equation is given by:

$$\begin{aligned} \dot{V} &= \int_0^{L_x} q_x(x,0)\dot{q}_x(x,0)dx + \int_0^{L_y} q_y(y,0)\dot{q}_y(y,0)dy \\ &+ \int_0^{L_x} M_x(x,0)\dot{M}_x(x,0)dx + \int_0^{L_y} M_y(x,0)\dot{M}_y(x,0)dx. \end{aligned} \tag{4.11}$$

By using Theorems 1 and 2, we obtain:

$$\dot{W} \leq \underset{u\in U}{inf}\,\underset{x\in Q}{sup}[x^2 + y^2] = \underset{u\in U}{inf}\,\underset{x\in Q}{sup}[2u_1y_1 + u_2y_2 + 2u_3y_3 + u_4y_4], \tag{4.12}$$

with $W = \dot{V}(x,y,t) - \alpha(x,y,t)$ and $\alpha = x^2 + y^2$. With these results, the robust passivity-based control law is established, and the proof of the theorem is complete.

□

The proof of the presented theorem provides sufficient conditions for stabilizing the uncertain Navier-Stokes equation in the port-Hamiltonian formulation. This fact is achieved by selecting an appropriate storage function to synthesize the passivity-based boundary controller. As verified, the uncertainties in this case are found in the boundary conditions, which makes it difficult for controller synthesis. However, this problem is tackled efficiently by selecting the appropriate robust storage function, so that boundary robust stability conditions are met. These conditions ensure that the waves shown in the numerical analysis section are suppressed efficiently.

From the application point of view, the results found by the previous theorem are helpful to obtain the wave suppression as found in the numerical wave tank as depicted in Figure 3. The proposed

robust boundary control strategy provides a sufficient control input that is later converted into the pump voltage to regulate the flow in the numerical wave tank.

In this way, the proposed robust boundary control strategy stabilizes the waves in the NWT and suppresses chaotic behavior, thereby protecting offshore renewable energy systems. As verified later in this research paper, the flow in the numerical wave tank is stabilized to protect a wave energy converter, to avoid damage to the WEC, and to suppress over-voltages.

5. Numerical wave tank for a wave energy converter

In this section, the numerical setup of the wave tank to be tested by a wave energy converter is presented. In this section, the following subsections are analyzed.

- Wave energy converter dynamics.
- Numerical setup of the numerical wave tank in Figure 3.
- Numerical experiments.

The main reason to establish this numerical setup is to test the wave energy converter under severe conditions, in order to stabilize the WEC and protect it from damage and destruction in its mechanical and electrical parts.

5.1. Wave energy converter dynamics

The wave energy converter dynamical behaviors are given by:

$$I\dot{\Omega} = \frac{P_{turb} - P_{gen}}{\Omega} + u, \tag{5.1}$$

where Ω is the angular velocity of the generator, I is the inertia of the generator, P_{turb} is the power of the turbine, and P_{gen} is the applied power [65]. The power generated by the turbine is [65, 66]:

$$P_{turb} = \rho_{in}\Omega^3 D^5 f_{\Pi}(\Psi), \tag{5.2}$$

where ρ_{in} is the air density in the turbine, D is the turbine generator diameter, and Ψ is given as [65,66]:

$$\Psi = \frac{\Delta p}{\rho_{in}\Omega^2 D^2}, \tag{5.3}$$

in which Δp is the pressure differential. Meanwhile, $f_{\Pi}(\Psi)$ is a non-dimensional function.

The control law u is basically a proportional-derivative controller considering the error variables $e_\Omega = \Omega - \Omega_d$ in which Ω is the velocity of the wave energy converter and Ω_d is the desired angular velocity. The PD controller is given by:

$$u = K_p e_\Omega + K_d \dot{e}_\Omega \tag{5.4}$$

with $K_p, K_d > 0$ being positive constants. The main variables are summarized in Table 3 and evinced in Figure 4:

Table 3. Variables of the wave energy converter

Variable	Definition	Type of variable
Ω	This variable is the angular velocity of the WEC's shaft.	Controlled variable
Ω_d	This variable is the angular velocity reference of the WEC's shaft. It is given by $\Omega_d = \|\|[q_x, q_y]\|\|$.	Reference variable
P_{turb}	This variable is the power of the turbine.	System variable
P_{gen}	This variable is the generated power of the WEC.	System variable
u	This variable is the control input of the WEC.	Manipulated variable

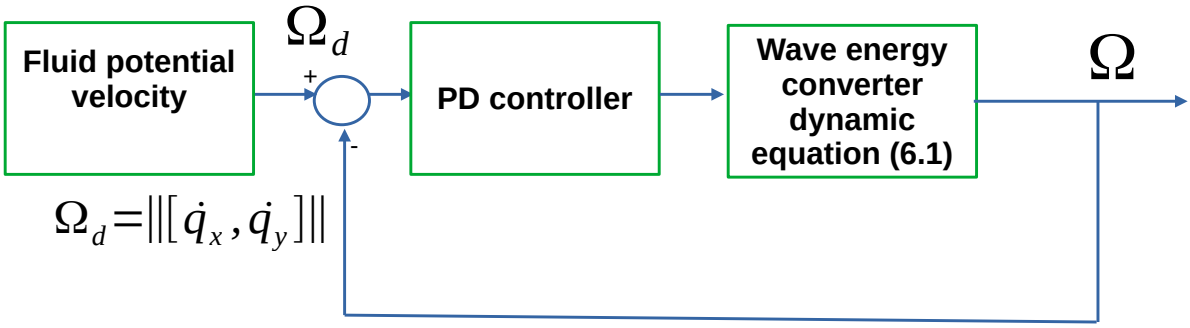

Figure 4. Block diagram of the control scheme of the wave energy converter.

As shown in Figure 4, the resultant of the velocity potential of the fluid $\Omega_d = \|\dot{q}_x, \dot{q}_y\|$ is the shaft angular velocity reference of the WEC. The primary reason is that the water velocity must be synchronized with the angular velocity of the shaft of the wave energy converter. In this way, when the chaotic vortex velocity is stabilized, the wave energy converter's angular shaft velocity is diminished smoothly to keep the WEC in safer operation until the water velocity is reduced to zero.

6. Numerical dynamic analysis and experiments

6.1. Dynamic analysis of the uncertain chaotic 2D Navier-Stokes equation

To find the eigenfunction of the Navier-Stokes equation along with the respective eigenvalues, the following separation of variables must be considered:

$$\begin{aligned} u_x &= T(t)X(x,y), \\ u_y &= T(t)Y(x,y). \end{aligned} \tag{6.1}$$

So, the following partial derivatives are computed for u_x:

$$\frac{\partial u_x}{\partial t} = T'(t)X(x,y), \qquad \frac{\partial u_x}{\partial x} = T(t)X'(x,y), \tag{6.2}$$

$$\frac{\partial^2 u_x}{\partial x^2} = T(t)X''(x,t), \qquad \frac{\partial u_x}{\partial y} = T(t)\dot{X}(x,y), \tag{6.3}$$

$$\frac{\partial^2 u_x}{\partial y^2} = T(t)\ddot{X}(x,y), \tag{6.4}$$

and the following partial derivatives are computed for u_y:

$$\begin{aligned} &\frac{\partial u_y}{\partial t} = T'(t)Y(x,y), && \frac{\partial u_y}{\partial x} = T(t)Y'(x,y),\\ &\frac{\partial^2 u_y}{\partial y^2} = T(t)Y''(x,t), && \frac{\partial u_y}{\partial x} = T(t)\dot{Y}(x,y),\\ &\frac{\partial^2 u_y}{\partial x^2} = T(t)\ddot{Y}(x,y). \end{aligned} \tag{6.5}$$

Then, the eigenfuction is obtained from (3.1) by implementing the two previous equations:

$$\begin{aligned} \rho T'X + \rho TXTX' + \rho TYT\dot{X} = -\frac{\partial p}{\partial x} + \mu TX'' + \mu T\ddot{X} = -\lambda_1,\\ \rho T'Y + \rho TXT\dot{Y} + \rho TYTY' = -\frac{\partial p}{\partial y} + \mu T\ddot{Y} + \mu TY'' = -\lambda_2, \end{aligned} \tag{6.6}$$

in which λ_1 and λ_2 are the eigenvalues of the Navier-Stoke equation in 2D. By rearranging, the following eigenfunctions are obtained:

$$\begin{aligned} -\tfrac{1}{T}\tfrac{\partial p}{\partial x} + \mu\nabla^2.X - \rho\,(U.\nabla X) + \lambda_1 x = 0,\\ -\tfrac{1}{T}\tfrac{\partial p}{\partial y} + \mu\nabla^2.Y - \rho\,(U.\nabla Y) + \lambda_2 y = 0, \end{aligned} \tag{6.7}$$

with the following boundary conditions:

$$\begin{aligned} &u_x(L_x,t) = u_{xL0}, && u_y(L_y,t) = u_{yL0},\\ &u_x(0,t) = u_{xt0}, && u_y(0,t) = u_{yt0},\\ &u_x(x,0) = u_{t0x}, && u_x(y,0) = u_{t0y}. \end{aligned} \tag{6.8}$$

In Figure 5, the phase portraits of the chaotic vortices of the numerical wave tank are shown. In Figure 6, the evolution in time of the fluid velocity in the x- and y-axes, respectively, was given. These phase portraits were obtained at $x = 18\ m$ and $y = 8\ m$. We can observe the water waves generated in the numerical wave tank, which should be suppressed and controlled. In Figure 7, the evolution in time of the eigenvalues of the system is shown. It can be observed that these eigenvalues reach stability at $\lambda_1 = 0.5849$ and $\lambda_2 = -0.1998$. This fact indicates that the solution of the system is unstable under

these conditions. Therefore, in the next section, the system is stabilized to suppress the chaotic vortex of the Navier-Stokes equation in the port-Hamiltonian formulation.

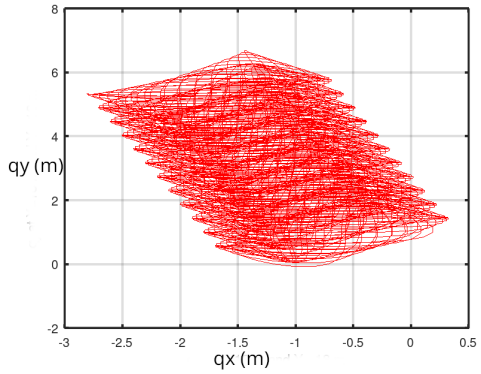

(a) Phase plot of q_x and q_y

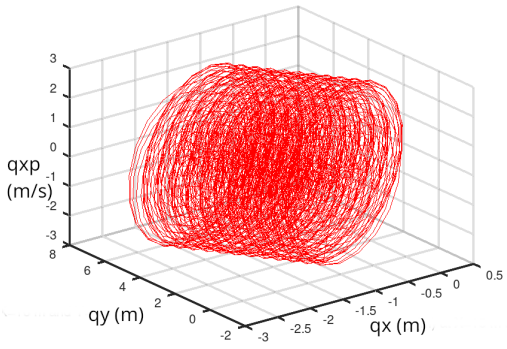

(b) 3D phase plot of q_x, q_y, and q'_x

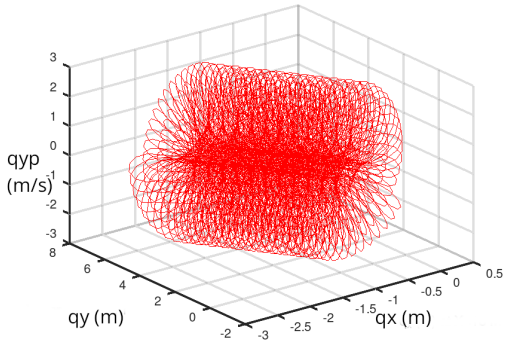

(c) 3D phase plot of q_x, q_y, and q'_y

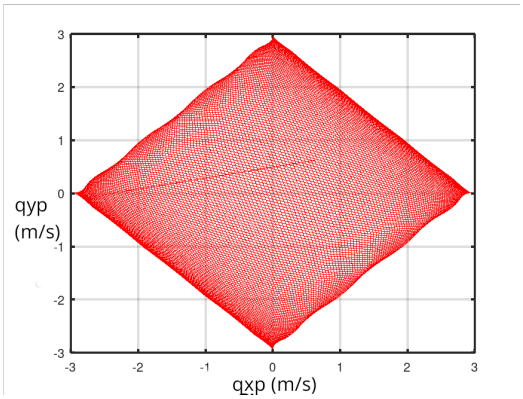

(d) Phase plot of q'_x and q'_y

Figure 5. Phase plots of the chaotic 2D Navier-Stokes equations.

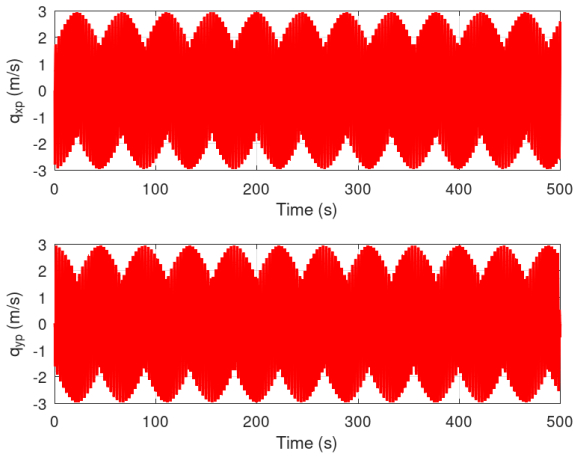

Figure 6. Evolution in time of q'_x and q'_y at $x = 8$ m and $y = 8$ m.

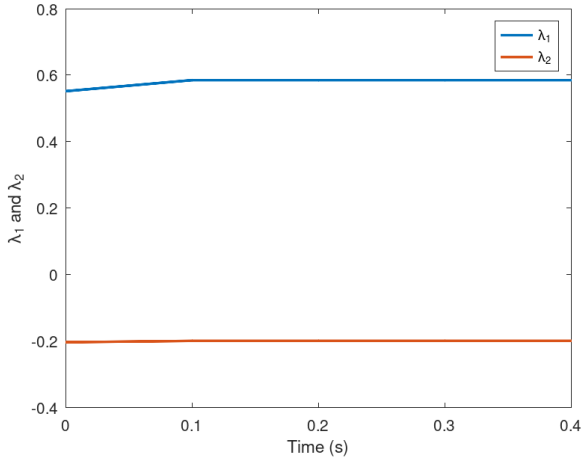

Figure 7. Eigenvalues of the numerical wave tank by solving the 2D Navier-Stokes equations.

Additionally, bifurcation diagrams and Lyapunov exponents are used to validate whether the Navier-Stokes uncertain formulation exhibits chaotic or hyper-chaotic behavior. Let us define the pressure vector of the Navier-Stokes equation as:

$$\begin{aligned} p_1 &= p_x \sin(X), \\ p_2 &= p_y \cos(Y). \end{aligned} \tag{6.9}$$

By selecting $p_y = 2 \times 10^{-5}$ while varying ρ, the bifurcation diagrams are obtained. In Figure 8, the bifurcation diagrams for the variables q_x, q_y, $\dot{q}_x$, and $\dot{q}_y$ are shown. It is verified that for the lowest values of the constant A, the solution of the Navier-Stokes equation in the port-Hamiltonian formulation converges to chaotic behavior, where the area in blue in the bifurcation diagrams corresponds to the chaotic regime.

The Lyapunov exponents are given in Table 4. Figure 9 shows the Lyapunov exponents with the respective evolution in time. It is noticeable that the real part of one Lyapunov exponent l_1 is positive, meanwhile the Lyapunov exponent l_2, l_3, and l_4 possess negative real parts, so the distributed parameter port-Hamiltonian system suggests a chaotic behavior.

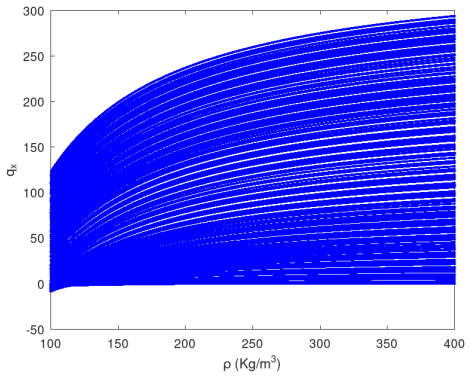

(a) Bifurcation diagram of q_x

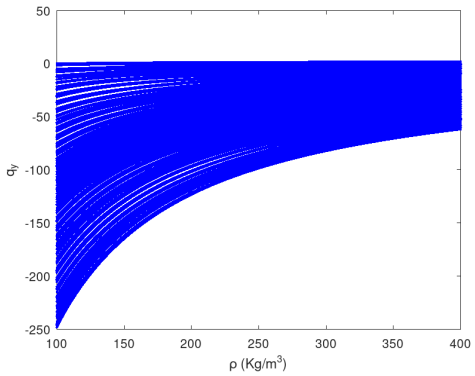

(b) Bifurcation diagram of q_y

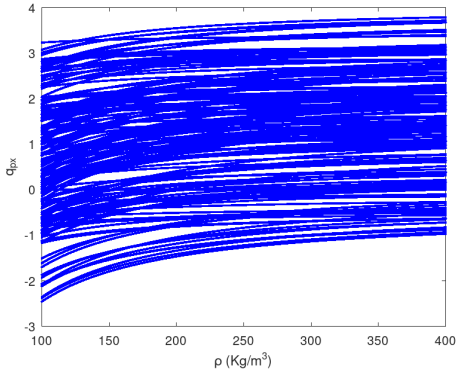

(c) Bifurcation diagram of q_x

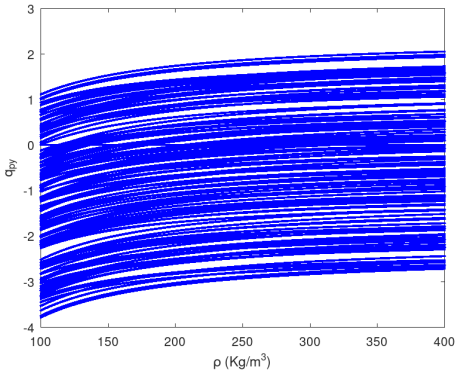

(d) Bifurcation diagram of q_y

Figure 8. Bifurcation diagrams for the variables q_x and q_y.

Table 4. Lyapunov exponents for the Navier-Stokes equation in the port-Hamiltonian form.

Lyapunov exponent	Value
l_1	7.5129×10^{-2}
l_2	-5.9064×10^{-3}
l_3	-1.5837×10^{-4}
l_4	-0.034605

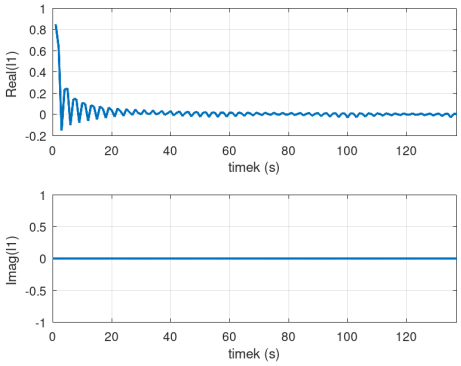

(a) Lyapunov exponent l_1

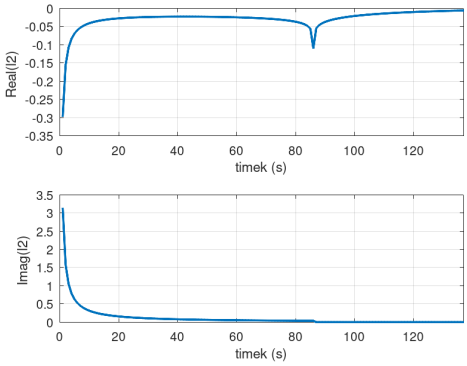

(b) Lyapunov exponent l_2

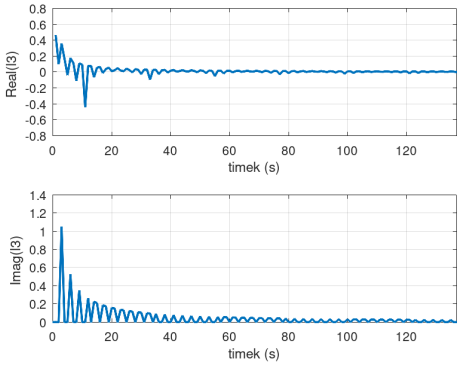

(c) Lyapunov exponent l_3

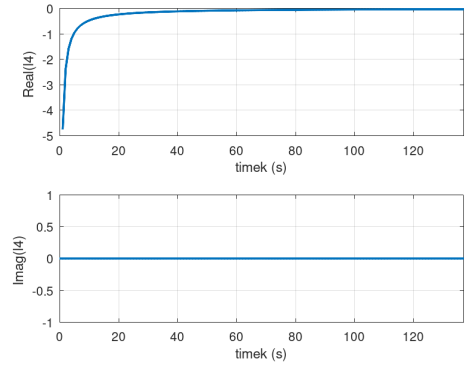

(d) Lyapunov exponent l_4

Figure 9. Evolution in time of the Lyapunov exponents.

6.2. Numerical experiment of the stabilization of the Navier-Stokes equation and the numerical wave tank

The numerical experiment consists of a simulation time of $t = 500\ s$, meanwhile the parameters of the numerical wave tank are $\rho = 1000\ Kgm/m^3$ and $\mu = 1 \times 10^{-3}\ Pa.s$ for the water density and viscosity, respectively. The uncertainties are given as $\eta_1 = sin(x)$ and $\eta_2 = sin(y)$. In Figure 10, the mesh plot and the contour plot of the variable q_x are shown. As shown in that figure, it is noticeable that the variables are stabilized in comparison with the plots shown in Figures 1 and 2. The effect of the robust passivity-based controller evinces that this control strategy is effective for the stabilization and wave suppression in the numerical wave tank. The numerical method used to solve the Navier-Stokes equation in the port-Hamiltonian formulation employs the finite difference method. The scheme is very similar to the numerical method which appears in [27, 49, 54, 67–69], where the discretization scheme is given as:

$$(q_j)_t^n = \frac{q_j^{n+1} - q_j^n}{h}, \qquad (\dot{q}_j)_{yy}^n = \frac{\dot{q}_{j+1}^n - 2\dot{q}_j^n - \dot{q}_{j-1}}{\Delta y^2}, \qquad (\dot{q}_j)_{xx}^n = \frac{\dot{q}_{j+1}^n - 2\dot{q}_j^n - \dot{q}_{j-1}}{\Delta x^2}, \tag{6.10}$$

where $h = \Delta t$ [67]. The finite difference method for solving this numerical setup involves creating a 2D mesh and then calculating the first-order and second-order partial derivatives. In this case, system (4.6)

is represented in a numerical scheme in the following way:

$$q_j^{n+1} = q_j^n + h(q_j)_t^n, \tag{6.11}$$

and

$$\begin{aligned} \frac{\partial q}{\partial t} &= (q_j)_t^n, \\ \frac{\partial M}{\partial t} &= \nabla p - \mu \begin{bmatrix} (\dot{q}_j)_{xx}^n \\ (\dot{q}_j)_{yy}^n \end{bmatrix} - \rho g. \end{aligned} \tag{6.12}$$

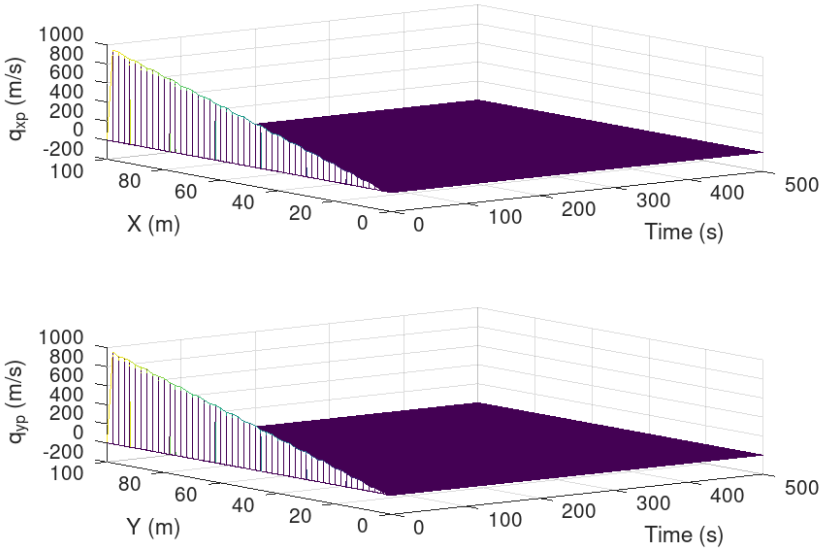

Figure 10. Plot of the variable q_x.

Therefore, to solve the previous scheme numerically, a mesh grid must be implemented to solve the Navier-Stokes problem with determined boundary conditions. The parameters of the wave energy converter are given as $R = 10\ m$, $J = 1 \times 10^9\ Kgm.m^2$, and rated power of $10\ MW$. The controller gains are given by $K_1 = 1 \times 10^{-5}$ and $K_2 = 1 \times 10^{-5}$ whereas the proportional and derivative gains of the wave energy converter are $K_p = 1 \times 10^{-1}$ and $K_d = 1 \times 10^{-1}$.

In Figure 11, the evolution in time of the input variables of the proposed control strategy is shown. It is verified how these input variables drove the position and velocity variables of the fluid to the equilibrium. In Figure 12, the evolution in time of how the velocities of the fluid in the x- and y-axes are driven to the equilibrium in finite time is shown. In Figure 13, the evolution of the variable P_m, which is the measured power of the wave energy converter, is displayed. As illustrated, this variable is maintained in a safe region because it remains below the rated power when the wave is suppressed.

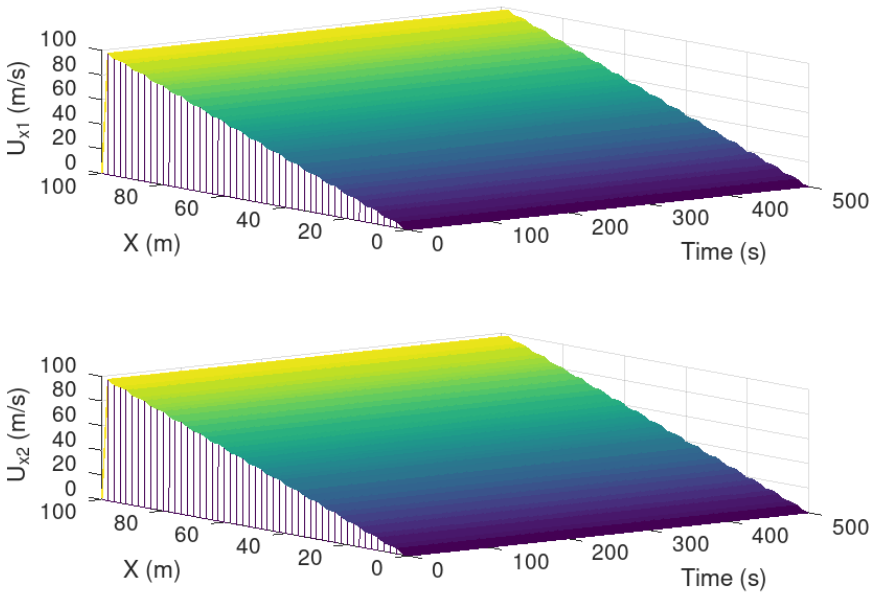

Figure 11. Input variables u_{x1} and u_{x2}.

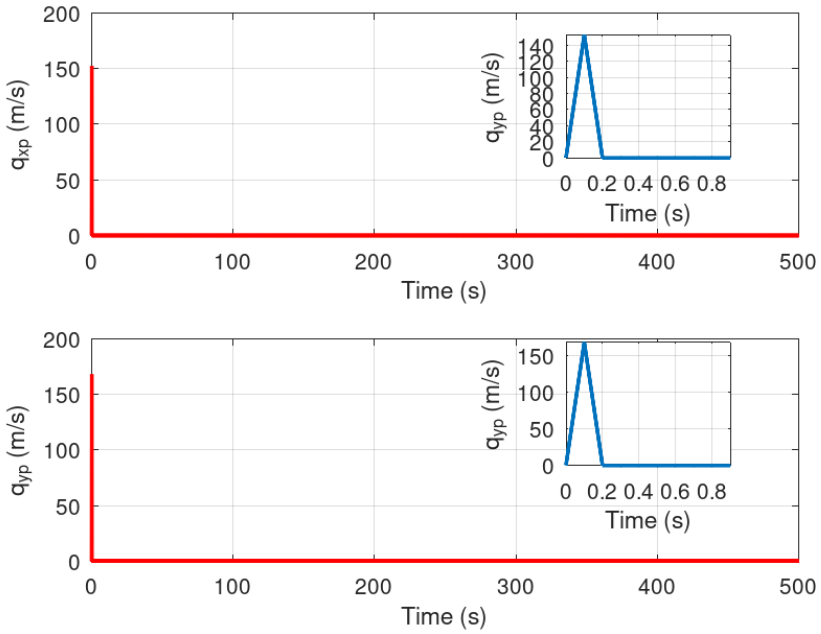

Figure 12. Evolution in time of q'_x and q'_y at $x = 8\ m$ and $y = 8\ m$.

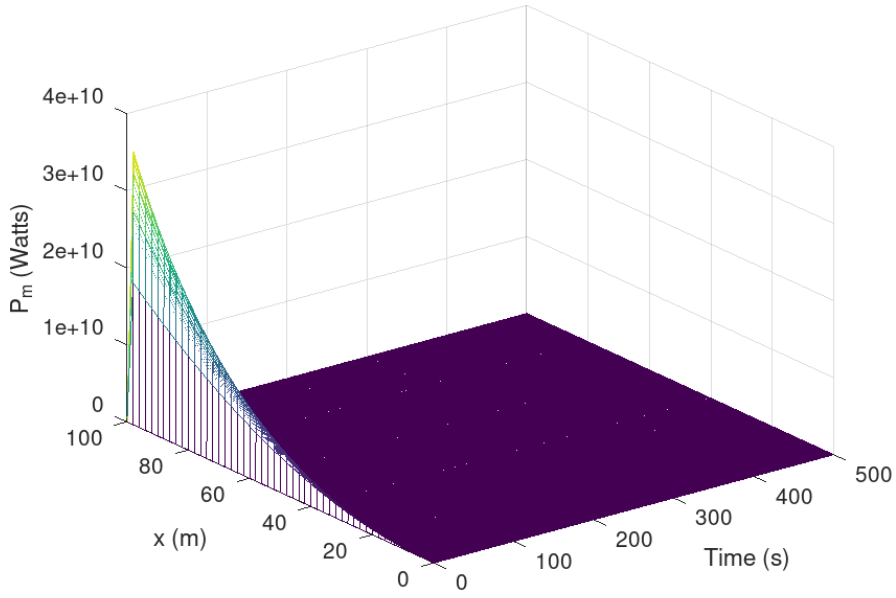

Figure 13. Plot of the variable P_m.

Also, in Figures 14 and 15, the evolution in time of the angular velocity ω and the error velocity e_Ω are shown, respectively. In the first case, this variable reaches stability due to wave suppression in the numerical wave tank. The error variable $e = \Omega - \Omega_d$ converges rapidly to the origin due to the action of the robust passivity-based boundary controller.

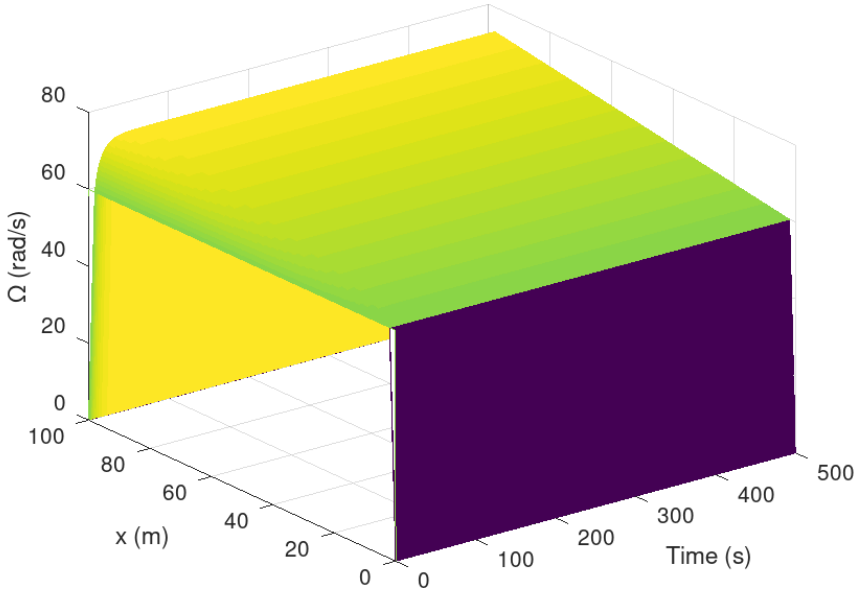

Figure 14. Plot of the variable Ω.

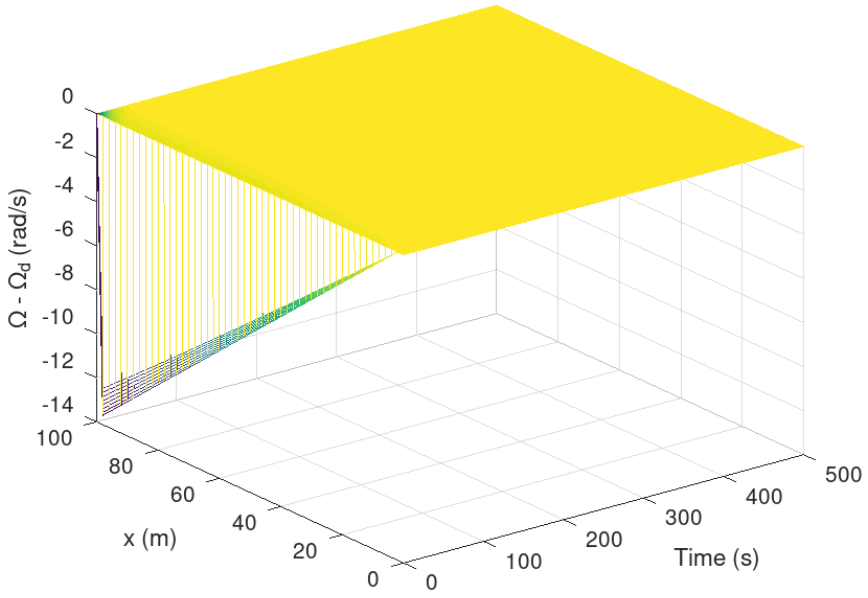

Figure 15. Plot of the error variable $e = \Omega - \Omega_d$.

Finally, in this subsection, a robustness analysis is performed considering the following boundary conditions:

$$\begin{aligned} \dot{q}_x &= -K\sin(x), \\ \dot{q}_y &= K\sin(y). \end{aligned} \tag{6.13}$$

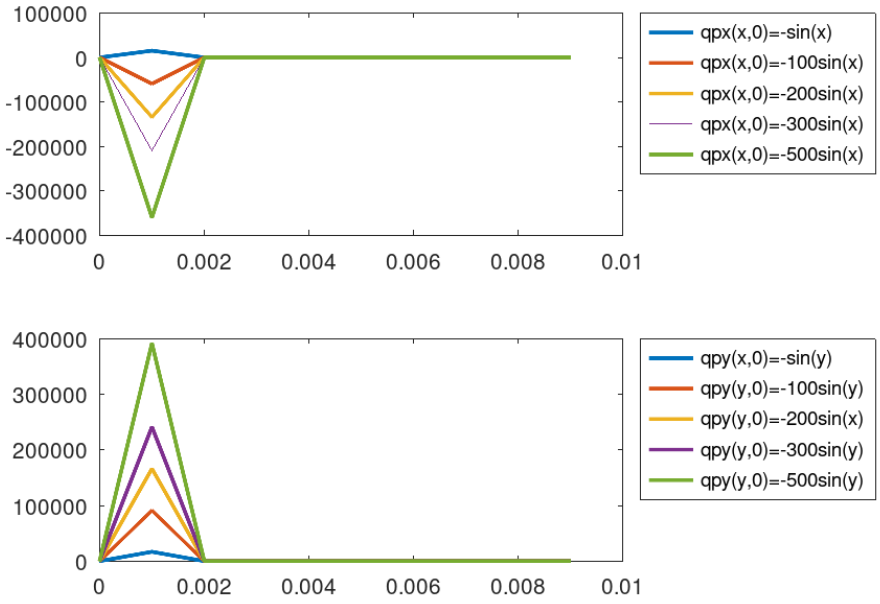

Figure 16. Robustness analysis while varying the constant K.

This robustness analysis consists of varying the constant value K in the values $K = 1, 100, 200, 300, 500$ to observe how the stabilization is performed under different boundary conditions. It is observed in Figure 16 how the stabilized variables vary according to the changes in the boundary conditions. It is evident that at low constant values, the overshoot is small; however, as the constant K increases, the overshoot in the stabilized variables increases.

7. Discussion

As explained in this paper, the primary objective of this study is to suppress wave-induced chaotic vortices in a wave energy converter system. Despite the chaotic vortex, this phenomenon is efficiently suppressed, thereby allowing the wave energy converter to remain in a safe region. For this reason, it is essential to note that the power is maintained at a secure range while simultaneously keeping the angular velocity of the wave energy converter at an appropriate level to prevent blade damage. The results regarding the passivity-based controller action demonstrate that the chaotic vortex is suppressed, enabling the wave energy converter to remain in a safe region. It is essential to clarify that the measured power in the wave energy converter is not maintained at the rated power, as the objective of this study is to ensure safe operation. As a future direction, a maximum power point tracking algorithm will be developed.

The answers to the hypothesis established in the introduction section are given as follows. In this case, based on the computed Lyapunov exponents, the system is classified as chaotic. More than two Lyapunov exponents possess positive real parts. Therefore, the bifurcation diagrams show when the system is in a chaotic regime, as evinced in Figure 8. Meanwhile, the eigenvalues of the original Navier-Stokes equations result in one positive and one negative eigenvalue. It is also shown that the robust passivity-based boundary controller stabilizes the optimal uncertain Navier-Stokes equation as a port-Hamiltonian system. Finally, the robust passivity-based boundary controller suppresses the chaotic behavior of the port-Hamiltonian system and protects the wave energy controller.

It is worth clarifying that the dynamic analysis is performed in the coordinates $x = 8\ m$ and $y = 8\ m$, obtaining similar results in the rest of the uncertain Navier-Stokes domain. One of the most important findings is that a hyper-chaotic attractor is found in all the domains of the uncertain Navier-Stokes equation. The turbulent chaotic vortex is found to necessitate an appropriate boundary control strategy to suppress chaotic behavior, maintain the wave energy converter's optimal performance, and simultaneously protect the mechanical and electrical integrity of the wave energy converter when chaotic vortices can damage or even destroy it.

Besides, the primary objective of the proportional-derivative controller of the wave energy converter is to maintain the angular velocity of the WEC according to the velocity potential of the water contained in the numerical wave tank. In this way, the velocity potential norm serves as the reference angular velocity for the wave energy converter, enabling it to achieve the required velocity in accordance with the fluid velocity. It is noticeable that the PD controller for the wave energy converter is sufficient to stabilize the angular velocity of the wave energy converter according to the water velocity potential, thereby stabilizing and protecting the WEC under turbulent, chaotic flow.

8. Conclusions

In this paper, a robust passivity-based boundary controller for a chaotic vortex in a numerical wave tank was proposed to protect a renewable wave energy converter. It has been proven both theoretically and numerically that such a controller efficiently suppresses a chaotic fluid vortex, thereby keeping a wave energy converter safe. The passivity-based boundary controller was designed using an appropriate storage function, similar to the lumped-parameter version. The uncertain Navier-Stokes equation was reformulated as a port-Hamiltonian system to develop a passivity-based boundary controller for wave suppression. For the wave energy converter, a proportional-derivative controller was sufficient to stabilize the WEC while maintaining an appropriate angular velocity until the wave is suppressed. The robust passivity-based boundary controller has been theoretically and experimentally validated; it is an effective technique for eliminating and suppressing chaotic behavior to protect the wave energy converter. This strategy is appropriate, given that the Navier-Stokes equations are formulated in the port-Hamiltonian approach, which enables exploitation of the energy properties inherent to this formulation. The stabilization technique performed efficiently, and, given that it is a relatively simple boundary control strategy from a theoretical standpoint, it is appropriate for chaos suppression in a real experimental setup.

The advantages of the proposed robust passivity-based control strategy are that the port-Hamiltonian formulation enables us to design the proposed control strategy with respect to input and output characteristics. Another advantage over other control techniques is that this control strategy accounts for matched uncertainties, which are commonly found in fluid and other physical systems. The disadvantages are that disturbances are not accounted for, a common feature of fluid systems. This issue will be considered as a future research direction.

As a future direction, this research study will be extended for a maximum power point tracking controller of the wave energy converter under smooth conditions. In this way, the controller can track the wave energy converter's rated power, enabling maximum power point tracking and power extraction even when the wave velocity field in the numerical wave tank is below the average. In this article, numerical wave tank simulations are conducted to maintain the wave energy converter in a safe region by suppressing the chaotic vortex, thereby protecting the WEC from damage or destruction.

Author contributions

Fernando E. Serrano: Conceptualization, methodology, software, validation, writing–original draft, review and editing; Vicenc Puig Cayuela: Conceptualization, methodology, software, validation, writing–original draft, review and editing; Jesus M. Munoz-Pacheco: Conceptualization, methodology, software, validation, writing–original draft, review and editing. All authors have read and agreed to the published version of the manuscript.

Use of Generative-AI tools declaration

The authors declare they have not used Artificial Intelligence (AI) tools in the creation of this article.

Acknowledgments

The third author acknowledges Benemérita Universidad Autónoma de Puebla for the support via the VIEP projects 2025–2026.

Conflict of interest

Prof. Jesus M. Munoz-Pacheco is the Guest Editor of special issue "Recent Advances in Chaotic System and Applications" for AIMS Mathematics. Prof. Jesus M. Munoz-Pacheco was not involved in the editorial review and the decision to publish this article.

The authors declare that they have no known competing financial interests or personal relationships that could have appeared to influence the work reported in this paper.

References

1. H. B. Yu, Global strong solutions and decay to the 3D full compressible Navier–Stokes equations without heat conductivity, *Discrete Cont. Dyn.-A*, **45** (2025), 1911–1927. https://doi.org/10.3934/dcds.2024152
2. C. Cavaterra, M. Grasselli, M. A. Mehmood, R. Voso, Analysis of a Navier–Stokes phase-field crystal system, *Nonlinear Anal.-Real*, **83** (2025), 104263. https://doi.org/10.1016/j.nonrwa.2024.104263
3. I. Herbst, Mild regularity of weak solutions to the Navier–Stokes equations, *Nonlinear Anal.-Theor.*, **254** (2025), 113744. https://doi.org/10.1016/j.na.2024.113744
4. Z. J. Tan, Y. H. Zeng, Temporal second-order two-grid finite element method for semilinear time-fractional Rayleigh–Stokes equations, *J. Comput. Appl. Math.*, **459** (2025), 116375. https://doi.org/10.1016/j.cam.2024.116375
5. M. Lukáčová-Medvid'ová, A. Schömer Conditional regularity for the compressible Navier-Stokes equations with potential temperature transport, *J. Differ. Equations*, **423** (2025), 1–40. https://doi.org/10.1016/j.jde.2024.12.028
6. S. Gao, Z. Y. Zhang, Q. Li, S. Q. Ding, H. H.-C. Iu, Y. H. Cao, et al., Encrypt a story: A video segment encryption method based on the discrete sinusoidal memristive Rulkov neuron, *IEEE T. Depend. Secure*, **22** (2025), 8011–8024. https://doi.org/10.1109/TDSC.2025.3603570
7. S. Gao, S. Q. Ding, H. H.-C. Iu, U. Erkan, A. Toktas, C. Simsek, et al., A three-dimensional memristor-based hyperchaotic map for pseudorandom number generation and multi-image encryption, *Chaos*, **35** (2025), 073105. https://doi.org/10.1063/5.0270220
8. S. Gao, R. Wu, H. H.-C. Iu, U. Erkan, Y. H. Cao, Q. Li, et al., Chaos-based video encryption techniques: A review, *Comput. Sci. Rev.*, **58** (2025), 100816. https://doi.org/10.1016/j.cosrev.2025.100816
9. W. G. Melo, L2 decay of weak solutions for the Navier–Stokes equations with supercritical dissipation, *Nonlinear Anal.-Real*, **84** (2025), 104329. https://doi.org/10.1016/j.nonrwa.2025.104329

10. J. H. Neyra, H. López-Lázaro, O. Rubio, C. R. T. Junior, Pullback exponential attractor of dynamical systems associated with non-cylindrical problems, *J. Math. Anal. Appl.*, **547** (2025), 129332. https://doi.org/10.1016/j.jmaa.2025.129332

11. A. Deeb, D. Dutykh, Numerical integration of Navier–Stokes equations by time series expansion and stabilized FEM, *Math. Comput. Simulat.*, **233** (2025), 208–236. https://doi.org/10.1016/j.matcom.2025.01.023

12. D. Wang, Z. F. Hao, F. Q. Chen, Y. S. Chen, Multi-mode motion dynamics of a top tensioned riser excited by vortices and varying tension, *Int. J. Bifurcat. Chaos*, **32** (2022), 2250144. https://doi.org/10.1142/S0218127422501449

13. B. H. Huynh, T. Tjahjowidodo, Experimental chaotic quantification in bistable vortex induced vibration systems, *Mech. Syst. Signal Pr.*, **85** (2017), 1005–1019. https://doi.org/10.1016/j.ymssp.2016.09.025

14. H. Zhang, B. B. Mao, H. Yang, J. J. Zhang, Modeling of coherent evolution of ocean turbulence based on time-dependent intrinsic correlation, *2023 IEEE 3rd International Conference on Power, Electronics and Computer Applications (ICPECA)*, Shenyang, China, 2023, 226–231. https://doi.org/10.1109/ICPECA56706.2023.10075883

15. Y. N. Aye, N. Srinil, Experimental observation on chaotic vortex-induced vibration of circular cylinder in turbulent flow, *2023 42nd International Conference on Ocean, Offshore and Arctic Engineering*, Melbourne, Australia, 2023, OMAE2023-101301. https://doi.org/10.1115/OMAE2023-101301

16. V. V. Zhmur, E. A. Ryzhov, K. V. Koshel, Ellipsoidal vortex in a nonuniform flow: dynamics and chaotic advections, *J. Mar. Res.*, **69** (2011), 435–461.

17. E. S. Baranovskii, E. Y. Prosviryakov, S. V. Ershkov, Mathematical analysis of steady non-isothermal flows of a micropolar fluid, *Nonlinear Anal.-Real*, **84** (2025), 104294. https://doi.org/10.1016/j.nonrwa.2024.104294

18. H. Kozono, S. Shimizu, Analyticity of solutions to the stationary Navier–Stokes equations via parameter trick, *Nonlinear Anal.-Real*, **84** (2025), 104319. https://doi.org/10.1016/j.nonrwa.2025.104319

19. F. L. Cardoso-Ribeiro, G. Haine, Y. L. Gorrec, D. Matignon, H. Ramirez, Port-Hamiltonian formulations for the modeling, simulation and control of fluids, *Comput. Fluids*, **283** (2024), 106407. https://doi.org/10.1016/j.compfluid.2024.106407

20. T. Reis, M. Schaller, Port-Hamiltonian formulation of Oseen flows, *Systems Theory and PDEs (WOSTAP 22 2022)*, Cham: Birkhäuser, 2024, 123–148. https://doi.org/10.1007/978-3-031-64991-2_5

21. M. Lohmayer, S. Leyendecker, Exergetic Port-Hamiltonian systems: Navier-Stokes-Fourier fluid, *IFAC-PapersOnLine*, **55** (2022), 74–80. https://doi.org/10.1016/j.ifacol.2022.08.033

22. G. Haine, D. Matignon, Incompressible navier-stokes equation as port-Hamiltonian systems: Velocity formulation versus vorticity formulation, *IFAC-PapersOnLine*, **54** (2021), 161–166. https://doi.org/10.1016/j.ifacol.2021.11.072

23. H. Fan, D. Y. Wu, Numerical investigation on vortex characteristics inside a jet pump under low entrainment ratio conditions, *Flow Meas. Instrum.*, **102** (2025), 102800. https://doi.org/10.1016/j.flowmeasinst.2024.102800

24. A. Khademi, E. Salari, S. Dufour, Simulation of 3D turbulent flows using a discretized generative model physics-informed neural networks, *Int. J. Nonlin. Mech.*, **170** (2025), 104988. https://doi.org/10.1016/j.ijnonlinmec.2024.104988

25. S. Zhong, C. Zhang, A. W. Fan. Numerical study on heat transfer enhancement of laminar flow in fully wavy wall microchannels, *Appl. Therm. Eng.*, **266** (2025), 125782. https://doi.org/10.1016/j.applthermaleng.2025.125782

26. J.-N. Zhang, S.-X. Wei, T.-L. Xie, H.-T. Tong, Q. Liu, S.-F. Yin. Hydrodynamic and mixing characteristics in oscillating feedback micromixers: influence of geometric configuration and scale, *Chem. Eng. Process.*, **209** (2025), 110153. https://doi.org/10.1016/j.cep.2025.110153

27. L. Li, P. Xu, Q. H. Li, Z. C. Yin, R. Y. Zheng, J. F. Wu, et al., Multi-field coupling particle flow dynamic behaviors of the microreactor and ultrasonic control method, *Powder Technol.*, **454** (2025), 120731. https://doi.org/10.1016/j.powtec.2025.120731

28. J. Redaud, J. Auriol, Y. L. Gorrec. In domain dissipation assignment of boundary controlled Port-Hamiltonian systems using backstepping, *Syst. Control Lett.*, **185** (2024), 105722. https://doi.org/10.1016/j.sysconle.2024.105722

29. S.-A. Hauschild, N. Marheineke, Model reduction for a Port-Hamiltonian formulation of the Euler equations, *Progress in Industrial Mathematics at ECMI 2021 (ECMI 2021)*, Cham: Springer, 2022, 1–7. https://doi.org/10.1007/978-3-031-11818-0_1

30. J.-P. Toledo-Zucco, D. Matignon, C. Poussot-Vassal, Y. L.Gorrec, Structure-preserving discretization and model order reduction of boundary-controlled 1D port-Hamiltonian systems, *Syst. Control Lett.*, **194** (2024), 105947. https://doi.org/10.1016/j.sysconle.2024.105947

31. A. MacChelli, Distributed-parameter Port-Hamiltonian systems in discrete-time, *2023 62nd IEEE Conference on Decision and Control (CDC)*, Singapore, Singapore, 2023, 2931–2936. https://doi.org/10.1109/CDC49753.2023.10383674

32. K. Y. Tan, P. L. Li, T. Beckers, Physics-constrained learning for PDE systems with uncertainty quantified Port-Hamiltonian models, *2024 6th Annual Conference on Learning for Dynamics and Control*, Oxford, UK, 2024, 1753–1764.

33. A. Macchelli, Y. L. Gorrec, Y. Wu, H. Ramírez, Energy-based control of a wave equation with boundary anti-damping, *IFAC-PapersOnLine*, **53** (2020), 7740–7745. https://doi.org/10.1016/j.ifacol.2020.12.1527

34. C. Ponce, H. Ramirez, Y. L. Gorrec, Finite dimensional shape control design of linear port-Hamiltonian systems with in-domain pointwise inputs, *IFAC-PapersOnLine*, **56** (2023), 6777–6782. https://doi.org/10.1016/j.ifacol.2023.10.385

35. N. Liu, Y. X. Wu, Y. L. Gorrec, L. Lefèvre, H. Ramirez, Reduced order in domain control of distributed parameter port-Hamiltonian systems via energy shaping, *Automatica*, **161** (2024), 111500. https://doi.org/10.1016/j.automatica.2023.111500

36. N. M. T. Vu, V. Trenchant, H. Ramirez, L. Lefèvre, Y. L. Gorrec, Parabolic matching of hyperbolic system using control by interconnection, *IFAC-PapersOnLine*, **50** (2017), 5574–5579. https://doi.org/10.1016/j.ifacol.2017.08.1101

37. N. Boonkumkrong, S. Chinvorarat, P. Asadamongkon, Passivity-based boundary control with the backstepping observer for the vibration suppression of the flexible beam, *Heliyon*, **9** (2023), e12740. https://doi.org/10.1016/j.heliyon.2022.e12740

38. M. R. J. Harandi, H. D. Taghirad, On the matching equations of kinetic energy shaping in IDA-PBC, *J. Franklin I.*, **358** (2021), 8639–8655. https://doi.org/10.1016/j.jfranklin.2021.08.034

39. P. Sozhaeswari, R. Sakthivel, M. Chadli, R. Abinandhitha, Design of fault-tolerant non-fragile control for parabolic PDE systems with semi-Markov jump: the finite-time case, *Int. J. Syst. Sci.*, **56** (2025), 2606–2623. https://doi.org/10.1080/00207721.2025.2450093

40. M. R. J. Harandi, S. A. Khalilpour, H. D. Taghirad, Adaptive energy shaping control of a 3-DOF underactuated cable-driven parallel robot, *IEEE T. Ind. Inform.*, **19** (2023), 7552–7560. https://doi.org/10.1109/TII.2022.3211980

41. R. D. Ayissi, G. Deugoué, J. N. Zangue, T. T. Medjo, On the existence of optimal and epsilon-optimal controls for the stochastic 2D nonlocal Cahn–Hilliard–Navier–Stokes system, *Nonlinear Analysis*, **265** (2026), 114016. https://doi.org/10.1016/j.na.2025.114016

42. S. Manservisi, F. Menghini, Numerical simulations of optimal control problems for the Reynolds averaged Navier–Stokes system closed with a two-equation turbulence model, *Comput. Fluids*, **125** (2016), 130–143. https://doi.org/10.1016/j.na.2025.114016

43. N. Smaoui, M. Zribi, Dynamics and control of the 2-d Navier–Stokes equations, *Appl. Math. Comput.*, **237** (2014), 461–473. https://doi.org/10.1016/j.amc.2014.03.150

44. Y. Zhou, L. Peng, Weak solutions of the time-fractional Navier–Stokes equations and optimal control, *Comput. Math. Appl.*, **73** (2017), 1016–1027. https://doi.org/10.1016/j.camwa.2016.07.007

45. C. Pozrikidis, Introduction to kinematics, In: *Fluid dynamics*, 3 Eds., New York: Springer, 2017, 1–62. https://doi.org/10.1007/978-1-4899-7991-9

46. A. Abbatiello, D. Basarić, N. Chaudhuri, On a blow-up criterion for the Navier–Stokes–Fourier system under general equations of state, *Nonlinear Anal.-Real*, **84** (2025), 104328. https://doi.org/10.1016/j.nonrwa.2025.104328

47. Y. R. Jin, X. L. Chen, Investigation into the reduction of aerodynamic drag via external windshields on high-speed trains, *J. Eng. Appl. Sci.*, **72** (2025), 7. https://doi.org/10.1186/s44147-025-00577-0

48. M. Y. Pan, C. X. Fu, L. Yang, D. D. He, A fully-decoupled, second-order accurate, positivity-preserving and energy stable scheme for a two-phase flow system with ions transport, *J. Comput. Appl. Math.*, **465** (2025), 116573. https://doi.org/10.1016/j.cam.2025.116573

49. C. Huang, H. X. Chen, Q. Cheng, L. J. Chen, Efficient positivity preserving schemes for stochastic complex systems, *J. Comput. Appl. Math.*, **462** (2025), 116464. https://doi.org/10.1016/j.cam.2024.116464

50. R. Rashad, S. Stramigioli, The Port-Hamiltonian structure of continuum mechanics, *J. Nonlinear Sci.*, **35** (2025), 35. https://doi.org/10.1007/s00332-025-10130-1

51. F. Califano, R. Rashad, F. P. Schuller, S. Stramigioli, Geometric and energy-aware decomposition of the Navier-Stokes equations: A port-Hamiltonian approach, *Phys. Fluids*, **33** (2021), 047114. https://doi.org/10.1063/5.0048359
52. N. Duan, Strong solution of 3D generalized Navier–Stokes equations with damping, *Bound. Value Probl.*, **2025** (2025), 40. https://doi.org/10.1186/s13661-025-01998-9
53. A. Novruzi, F. Mezatio, Existence and uniqueness of a time-periodic strong solution to incompressible Navier-Stokes equations in a time-periodic moving domain, describing the blood flow in an artificial heart, *J. Math. Anal. Appl.*, **548** (2025), 129410. https://doi.org/10.1016/j.jmaa.2025.129410
54. A. D. Polyanin, N. A. Kudryashov, Exact solutions and reductions of nonlinear Schrödinger equations with delay, *J. Comput. Appl. Math.*, **462** (2025), 116477. https://doi.org/10.1016/j.cam.2024.116477
55. S. Gao, Z. Y. Zhang, H. H.-C. Iu, S. Q. Ding, J. Mou, U. Erkan, et al., A parallel color image encryption algorithm based on a 2-D Logistic-Rulkov neuron map, *IEEE Internet Things*, **12** (2025), 18115–18124. https://doi.org/10.1109/JIOT.2025.3540097
56. S. Gao, H. H.-C. Iu, U. Erkan, C. Simsek, A. Toktas, Y. H. Cao, et al., A 3D memristive cubic map with dual discrete memristors: Design, implementation, and application in image encryption, *IEEE T. Circ. Syst. Vid.*, **35** (2025), 7706–7718. https://doi.org/10.1109/TCSVT.2025.3545868
57. Z. F. Ma, D. B. Tong, Q. Y. Chen, W. N. Zhou, Fixed/prescribed-time synchronization and energy consumption for Kuramoto-Oscillator networks, *IEEE T. Cybernetics*, **55** (2025), 3379–3389. https://doi.org/10.1109/TCYB.2025.3556103
58. M. Shi, D. B. Tong, Q. Y. Chen, W. N. Zhou, Pth moment exponential synchronization for delayed multi-agent systems with Lévy noise and Markov switching, *IEEE T. Circuits-II*, **71** (2024), 697–701. https://doi.org/10.1109/TCSII.2023.3304635
59. D. Gutiérrez-Oribio, I, Stefanou, F. Plestan, Passivity-based control of underactuated mechanical systems with Coulomb friction: Application to earthquake prevention, *Automatica*, **165** (2024), 111661. https://doi.org/10.1016/j.automatica.2024.111661
60. R. A. Freeman, P. V. Kokotovic, *Robust nonlinear control design: state-space and Lyapunov techniques*, Boston: Birkhäuser, 1996. https://doi.org/10.1007/978-0-8176-4759-9
61. A. Mironchenko, Lyapunov criteria for robust forward completeness of distributed parameter systems, *Syst. Control Lett.*, **180** (2023), 105618. https://doi.org/10.1016/j.sysconle.2023.105618
62. D. Gutiérrez-Oribio, Y. Orlov, I. Stefanou, F. Plestan, Robust boundary tracking control of wave PDE: Insight on forcing slow-aseismic response, *Syst. Control Lett.*, **178** (2023), 105571. https://doi.org/10.1016/j.sysconle.2023.105571
63. J. Auriol, F. Bribiesca-Argomedo, D. B. Saba, M. D. Loreto, F. D. Meglio, Delay-robust stabilization of a hyperbolic PDE–ODE system, *Automatica*, **95** (2018), 494–502. https://doi.org/10.1016/j.automatica.2018.06.033
64. A. Smyshlyaev, M. Krstic, Adaptive boundary control for unstable parabolic PDEs–Part II: estimation-based designs, *Automatica*, **43** (2007), 1543–1556. https://doi.org/10.1016/j.automatica.2007.02.014

65. B. Fenu, J. C. C. Henriques, M. Glorioso, L. M. C. Gato, M. Bonfanti, Real-time Wells turbine simulation on an oscillating-water-column wave energy converter physical model, *Appl. Energy*, **376** (2024), 124121. https://doi.org/10.1016/j.apenergy.2024.124121

66. S. Capasso, B. Tagliafierro, I. Martínez-Estévez, C. Altomare, M. Gómez-Gesteira, M. Göteman, et al., Development of an SPH-based numerical wave-current tank and application to wave energy converters, *Appl. Energy*, **377** (2025), 124508. https://doi.org/10.1016/j.apenergy.2024.124508

67. N. Jiang, H. H. Yang, A second order ensemble algorithm for computing the Navier-Stokes equations, *J. Math. Anal. Appl.*, **530** (2024), 127674. https://doi.org/10.1016/j.jmaa.2023.127674

68. M. Elghandouri, K. Ezzinbi, L. Saidi, Exploring well-posedness and asymptotic behavior in an Advection-Diffusion-Reaction (ADR) model, *J. Comput. Appl. Math.*, **462** (2025), 116465. https://doi.org/10.1016/j.cam.2024.116465

69. D. Černá, Orthogonal wavelet method for multi-stage expansion and contraction options under stochastic volatility, *Appl. Numer. Math.*, **212** (2025), 155–175. https://doi.org/10.1016/j.apnum.2025.02.001

AIMS Press